SIMULATION OF THE CERN GTS-LHC ECR ION SOURCE EXTRACTION SYSTEM WITH LEAD AND ARGON ION BEAMS

V. Toivanen*, G. Bellodi, D. Küchler, A. Lombardi, R. Scrivens, J. Stafford-Haworth,
CERN, Geneva, Switzerland

Abstract

A comprehensive study of beam formation and beam transport has been initiated in order to improve the performance of the CERN heavy ion injector, Linac3. As part of this study, the ion beam extraction system of the CERN GTS-LHC 14.5 GHz Electron Cyclotron Resonance Ion Source (ECRIS) has been modelled with the ion optical code IBSimu. The simulations predict self-consistently the triangular and hollow beam structures which are often observed experimentally with ECRIS ion beams. The model is used to investigate the performance of the current extraction system and provides a basis for possible future improvements. In addition, the extraction simulation provides a more realistic representation of the initial beam properties for the beam transport simulations, which aim to identify the performance bottle necks along the Linac3 low energy beam transport. The results of beam extraction simulations with Pb and Ar ion beams from the GTS-LHC will be presented and compared with experimental observations.

INTRODUCTION

Linac3 delivers the heavy ion beams for the CERN experimental programme and is the first section of the LHC (Large Hadron Collider) heavy ion injector chain. The subsequent accelerator chain utilizing the heavy ions from Linac3 is comprised of LEIR (Low Energy Ion Ring), PS (Proton Synchrotron), SPS (Super Proton Synchrotron) and ultimately the LHC.

The heavy ion beams are produced with the GTS-LHC 14.5 GHz room temperature ECR ion source [1] at an initial energy of 2.5 keV/u. The beams are accelerated with an RFQ to 250 keV/u, followed by an Interdigital-H Drift Tube Linear Accelerator (IH-DTL) to reach the final Linac3 output energy of 4.2 MeV/u. Downstream from the IH-DTL the beam is transported through a carbon foil stripper and a filter line to produce and separate the desired ion species for LEIR injection.

The GTS-LHC is based on the original Grenoble Test Source (GTS) developed at CEA [2, 3]. It has been used predominantly in afterglow mode to produce intense lead ion beams with $^{208}Pb^{29+}$ being the ion of choice since 2007. The normal operation is performed with 10 Hz repetition rate and 50 ms RF heating pulse length. A 200 μs long ion beam pulse is selected from the ~ 1 ms afterglow peak exhibited by the lead beam and accelerated at up to 5 Hz repetition rate through Linac3. Finally, the beam is stripped to $^{208}Pb^{54+}$ for LEIR injection. Following the beam development and testing performed in 2013 [4], the GTS-LHC will deliver $^{40}Ar^{11+}$ beam for fixed target experiments in 2015.

As a part of the LHC luminosity upgrade for ions, a comprehensive study of Linac3 beam formation and transport has been initiated. The first part of this study includes detailed modelling of Linac3 beam dynamics with simulations, starting from beam extraction from the GTS-LHC. The extraction simulations serve two distinct purposes. Firstly, a reliable modelling of the beam transport along Linac3 requires realistic initial beam definitions, which recreate the characteristic properties of ECRIS beams that are observed experimentally. With a realistic model of Linac3 the factors limiting the beam transport performance can then be identified and possibly remedied. Secondly, the optimization of the beam extraction itself has the potential to yield performance improvement.

The current state of beam dynamics studies is presented for Pb and Ar beams. The Ar beam has been chosen due to its availability for measurements in 2014 during the injector chain commissioning and preparation for the 2015 physics experiments.

EXTRACTION SIMULATIONS

Extraction Simulation Settings

The GTS-LHC ion beam extraction has been modelled with the ion optical code IBSimu [5]. The code provides good capabilities to simulate multispecies extraction from plasma in the presence of strong magnetic fields and space charge, conditions which are closely associated with ECR ion sources. Although the nonlinear positive plasma model used by the code [6] considerably simplifies the complex ECRIS plasma conditions, previous studies have shown that IBSimu is a powerful tool in modelling ECRIS extraction systems [7].

The GTS-LHC extraction geometry, presented in Fig. 1, includes a plasma electrode, an intermediate electrode and a grounded electrode, forming a triode extraction system. Downstream from the electrodes the extraction region opens into a vertical cylindrical pumping chamber, followed by a beam pipe section with an inner diameter of 65 mm. The simulations have been performed in 3D with coordinate x denoting the optical axis and z and y the transverse directions. The 3D magnetic field map of the GTS-LHC was calculated with Cobham Opera 3D simulation software [8] and it includes the solenoid and the permanent magnet hexapole fields. In addition, the field of the first beam line solenoid downstream from the extraction region is included in the simulations. The resulting longitudinal magnetic field pro-
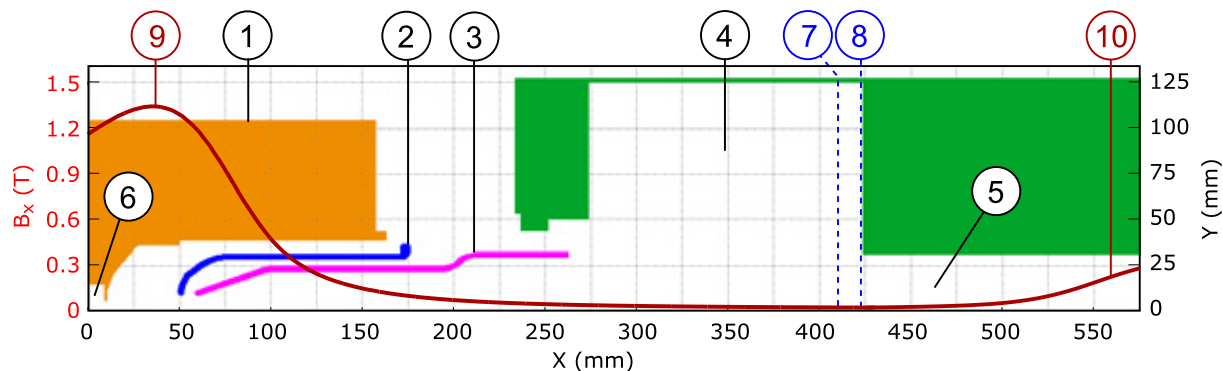
* ville.aleksi.toivanen@cern.ch

Figure 1: The GTS-LHC extraction geometry used in the simulations and the longitudinal magnetic field (B_x) profile on axis. The extraction system includes the plasma electrode (1), the intermediate electrode (2) and the grounded electrode (3), followed by the pumping chamber (4) and 65 mm diameter beam pipe (5). The plasma is modelled in a reduced volume (6). The locations of transverse beam observations are also indicated (7 and 8). The longitudinal magnetic field includes the ECRIS solenoid field (9) and the field of the first beam line solenoid (10).

file on axis is presented in Fig. 1 superimposed over the simulation geometry.

The afterglow discharge is characterized by the collapse of the electron population due to the loss of confinement by the RF field and the subsequent burst of extracted ions [9]. In the simulation this is modelled by assuming an increased plasma potential of 200 V, about an order of magnitude higher than is usually measured for second generation ECR ion sources in CW mode [10, 11], and a low 10 eV temperature for the cold background electron population. A cold ion population was assumed with longitudinal and transverse temperatures of 1 eV based on the generally accepted order of magnitude in ECR plasmas [12] and discretized into $\sim 1.4 \cdot 10^6$ tracked macro particles. The initial ion species distributions were defined based on the measured charge state distributions (CSD). The ion species dependent losses in the extraction region, caused by the influence of the strong magnetic field, were accounted for by iteratively adjusting the initial distribution to match the simulated CSD of the beam leaving the extraction region to the measured CSD. The simulation assumes full space charge in the extraction region. This is justified by the presence of strong electric fields preventing the accumulation of low energy compensating electrons into the beam potential. In addition, the compensation is mitigated by the low residual gas pressure in the extraction region (low 10^{-8} mbar region) and pulsed operation, which limit the electron production and accumulation time.

Three different cases have been studied with simulations; extraction of a Pb ion beam with the ion source tuned for the production of $^{208}Pb^{27+}$ and $^{208}Pb^{29+}$ and extraction of an Ar beam with the ion source tuned for the production of $^{40}Ar^{11+}$. The $^{208}Pb^{29+}$ case corresponds to the current Pb operation settings of the GTS-LHC and is the main case in order to improve the future Pb operation of Linac3. However, the beam is not available for experiments until 2015. In order to compare Pb operation with available experimental data, the earlier operation conditions with $^{208}Pb^{27+}$ were

simulated. The $^{40}Ar^{11+}$ case corresponds to the Ar operational settings that will be used for the 2015 fixed target physics experiments, and was modelled due to the availability of the Ar beam for experiments during the later half of 2014.

The Pb simulations are based on operational settings of the GTS-LHC at CERN. The Ar simulations are based on tests performed with the GTS-LHC at CERN [4] and the GTS2 at iThemba LABS [13]. The Pb beams are produced with oxygen mixing gas (included in the simulated CSD) whereas the Ar beam is produced with pure argon plasma. The extraction electrode voltages and other details are presented in Fig. 2 showing the simulations results.

Extraction Simulation Results

The simulated particle trajectory densities of the extracted Pb and Ar beams are presented in Fig. 2. In the case of the Pb beams the meniscus forms a convex shape, resulting to extraction of an initially diverging beam. The electric field and the axial magnetic field maximum in the acceleration gap provide strong charge-over-mass dependent focusing effect, yielding a beam waist inside the grounded electrode and separation of the beam envelopes of different ion species. With the argon beam the meniscus has a flat shape, which mitigates these effects and results into initially parallel beam extraction and more uniform particle distribution in the transverse plane (see Fig. 4). Due to the lack of additional focusing elements in the extraction region, in all simulated cases the beams are strongly divergent as they leave the grounded electrode, resulting in significant beam collimation against the walls of the extraction pumping chamber and the following beam pipe walls. With the Pb beams the simulations also show beam collimation at the intermediate electrode face and the inside of the grounded electrode. Visual inspection of the GTS-LHC extraction system shows clear beam induced markings at these locations. As an example, Fig. 3 presents a comparison of the simulated beam profile on the extraction pumping chamber wall (location 8
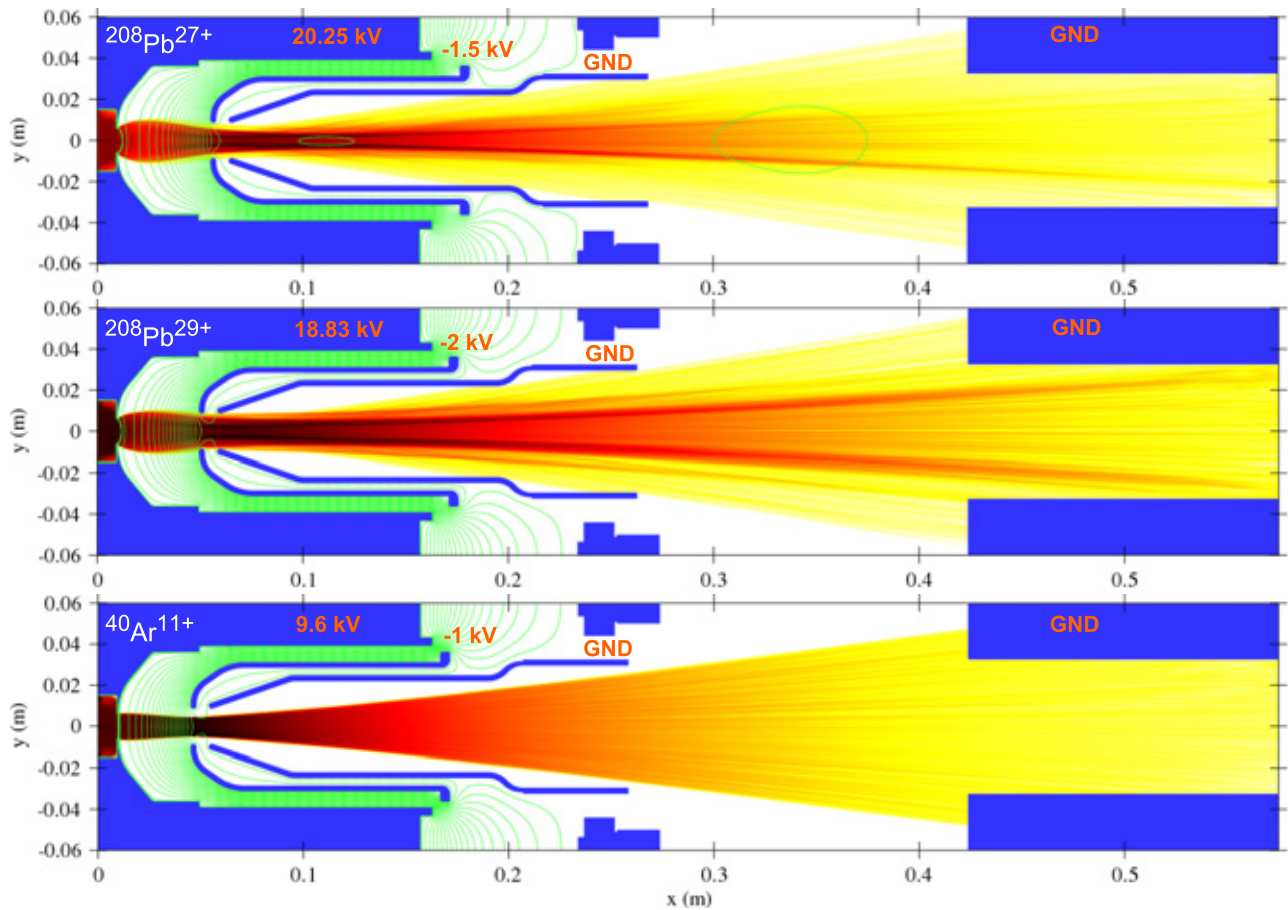
Ion beam extraction and optics

Figure 2: Simulated ion trajectory densities of the three studied cases through the GTS-LHC extraction region. The total extracted ion currents and acceleration gap lengths are: 3.5 mA and 45 mm for the $^{208}Pb^{27+}$ case, 5 mA and 40 mm for the $^{208}Pb^{29+}$ case and 1.6 mA and 35 mm for the $^{40}Ar^{11+}$ case.

in Fig. 1) and the beam induced markings observed at the same location. However, it is noted that the simulation only corresponds to the beam extraction during the afterglow, which constitutes only part of the extracted ion beam pulse. The extracted beam preceding the afterglow burst has different beam properties and can also contribute to the observed markings.
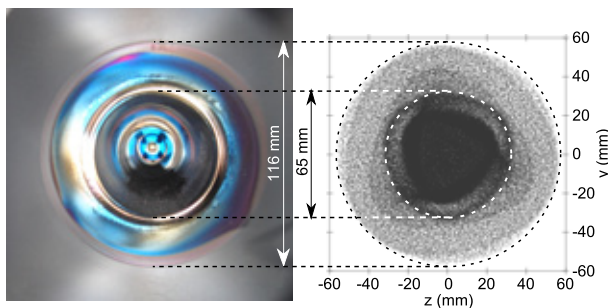

Figure 3: Comparison of the simulated beam particle positions (right) and experimentally observed beam induced markings (left) at the wall of the extraction pumping chamber.

The beam profiles of the total beams (all extracted ion species) and separately the ion species of interest ($^{208}Pb^{27+}$, $^{208}Pb^{29+}$ and $^{40}Ar^{11+}$) are presented in Fig. 4 at axial location $x = 414$ mm (location 7 in Fig. 1). The beams exhibit triangular shapes, which are the signature influence of the ECRIS magnetic confinement structure combining hexapole and solenoid fields. In addition, the Pb beams exhibit hollow beam structures and the formation of low intensity beam halo and triangular "wings", which are associated with the strong over-focusing inside the grounded electrode (for experimental examples of over-focused beam profiles, see e.g. [14]). These features are often experimentally observed with ion beams produced with ECR ion sources and are produced self-consistently by the simulation model. Due to the different initial extraction conditions avoiding the strong initial (over-) focusing inside the extraction electrodes, the transverse particle distribution of the Ar beam is significantly more uniform and exhibit very little aberrations compared to the Pb beams.

LEBT SIMULATIONS

The extraction simulation results presented in the previous section are used as initial beam definitions for the fol-
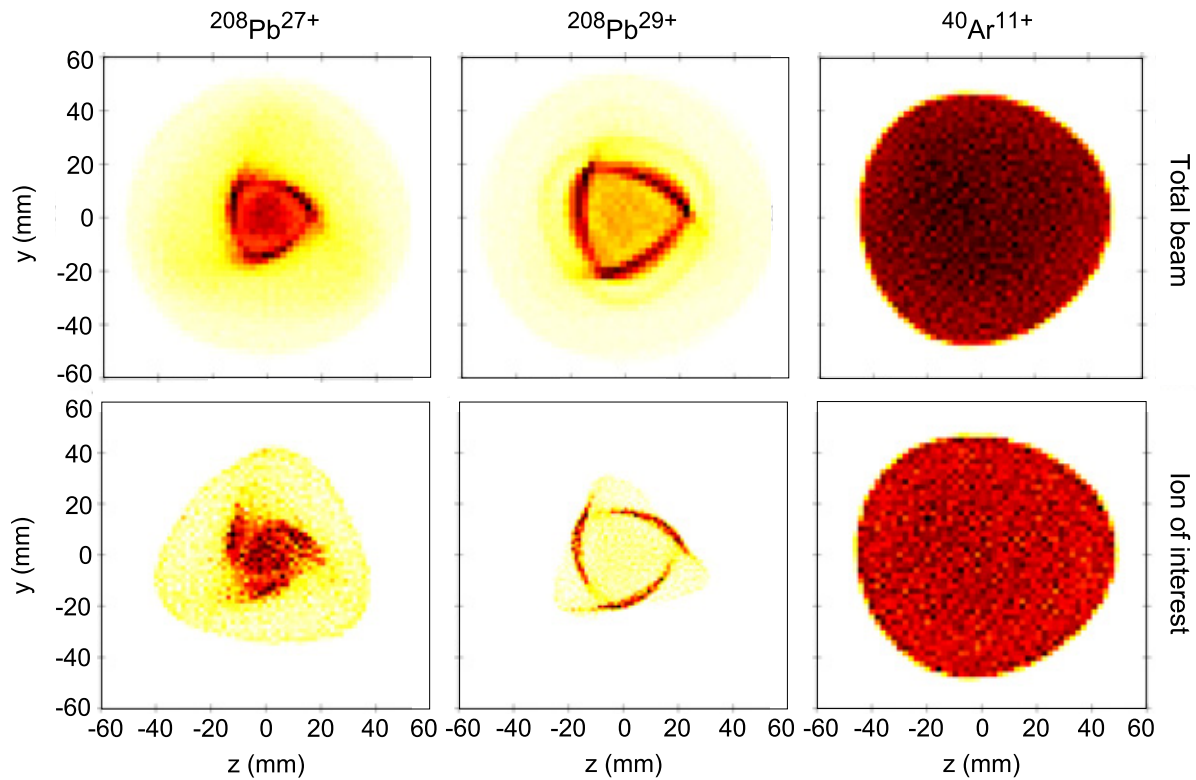
Figure 4: Simulated beam profiles of the three studied cases at the location 7 shown in Fig. 1 (see also Fig. 5). The upper row shows the profile of the full beam (all extracted ion species) and the lower row the profiles of the ion species of interest.
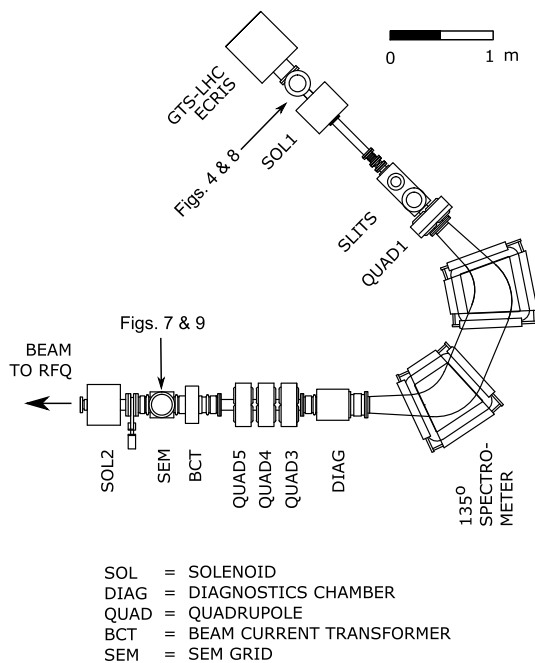
Figure 5: Linac3 LEBT with the main beam line components. The diagnostics chamber houses a horizontal slit, a Faraday cup (FC2) and in future a pepperpot emittance meter. The locations of the transverse beam diagnostics (simulated and measured) presented in the other figures are also indicated.

lowing beam dynamics simulations of the Linac3. This is an on-going study and consequently the discussion here will be limited to the first preliminary results of the low energy beam transport (LEBT) section of Linac3, the schematic of which is presented in Fig. 5. A detailed model of the Linac3 LEBT was constructed with the 3D multiparticle tracking code PATH [15]. To achieve a realistic representation of the beam transport, the machine elements are modelled based on their measured properties with operational settings and beam losses are calculated with a realistic aperture model.

The simulated transmission of $^{208}Pb^{27+}$ ion beam through the LEBT is presented in Fig. 6. As was observed in the extraction simulations, significant amount of the initial extracted beam is collimated at the end of the extraction region before reaching the first beam line solenoid. As a result, Over 60 % of the total extracted beam and about half of the $^{208}Pb^{27+}$ beam is lost during the first 0.3 m of beam transport. Apart from this initial collimation, the $^{208}Pb^{27+}$ does not exhibit further significant beam losses until near the end of the LEBT, yielding ∼ 40 % transmission to the RFQ. The other ion species experiencing suboptimal focusing are collimated during beam transport, steadily decreasing the transmission of the total beam, until the last of them are eliminated at the slit downstream from the spectrometer. Similar trends are observed with the other beams from the extraction simulations.

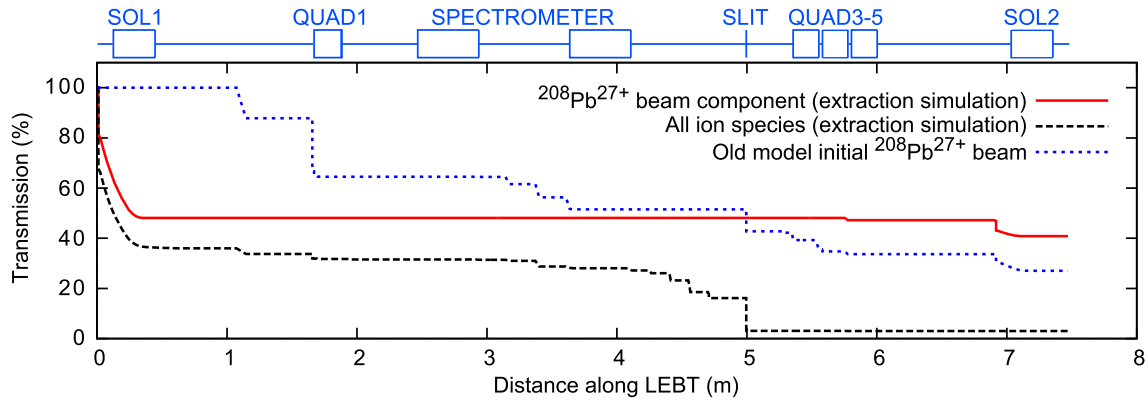Comparison of simulated and measured beam properties of $^{40}Ar^{11+}$ and $^{208}Pb^{27+}$ beams downstream from the Linac3

Figure 6: The simulated transmission through the Linac3 LEBT with the $^{208}Pb^{27+}$ initial beam. Location $x = 0$ m corresponds to location 7 in Fig. 1. The main LEBT beam line elements are also shown (see Fig. 5).

Table 1: Comparison of simulated and measured beam properties of $^{40}Ar^{11+}$ and $^{208}Pb^{27+}$ beams downstream from the Linac3 spectrometer. The results with the initial beam used by the old Linac3 model is also presented. $P_{rms}^{x,y}$ denotes the transverse rms beam profile widths and $\epsilon_{rms}^{x,y}$ the rms emittance in the (x,x') and (y,y') phase spaces.

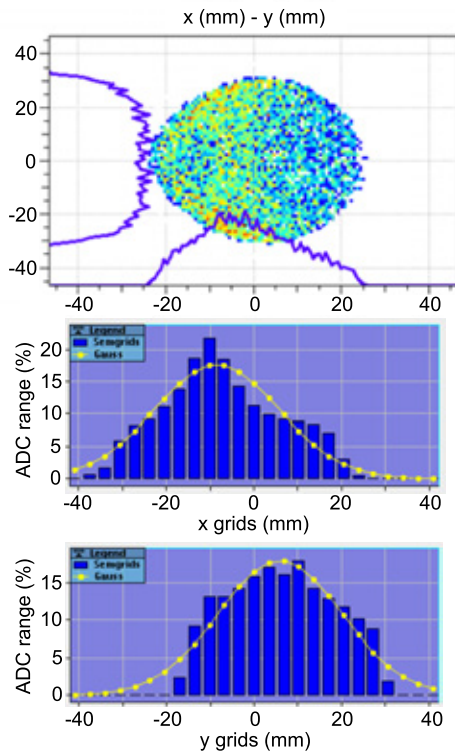|	P_{rms}^{x} (mm)	P_{rms}^{y} (mm)	ϵ_{rms}^{x} (mm mrad)	ϵ_{rms}^{y} (mm mrad)
$^{40}Ar^{11+}$ simulated	11	16	38	18
$^{40}Ar^{11+}$ measured	14	14	-	-
$^{208}Pb^{27+}$ simulated	9	11	30	28
$^{208}Pb^{27+}$ measured	7	7	39 ± 4	29.9 ± 0.4
$^{208}Pb^{27+}$ old model	25	12	320	118

Figure 7: Comparison of simulated and measured $^{40}Ar^{11+}$ beam profiles at the LEBT SEM grid (see Fig. 5).

spectrometer are presented in Table 1. Figure 7 presents the simulated $^{40}Ar^{11+}$ beam profile at the LEBT SEM grid compared with the measured profiles. Although the simulated and measured values are not identical, the simulated beam properties are in reasonable agreement with the measurements. Especially the simulated beam profile shape in Fig. 7 exhibits many of the same features as the measured profile.

The properties of the initial beam description used in the ion optics calculations have high impact on the simulation results. This is demonstrated in Figs. 8 and 9, which show the difference between using an initial beam distribution obtained from the presented extraction simulations ($^{208}Pb^{27+}$ case) and using the idealized initial beam definition for $^{208}Pb^{27+}$ that was originally used to design the Linac3 beam transport. Both cases have been simulated using the operational LEBT settings which experimentally yield the highest performance. It is observed that combining the old initial beam definition with the new 3D multiparticle beam transport model results in strong emittance blow-up during transport. This is caused by mismatch between the beam properties and the ion optical settings of the beam transport leading to cumulative emittance growth in the beam line focusing elements and the spectrometer. The incompatibility is also reflected in the beam losses occurring along the LEBT, as presented in Fig. 6. This underlines the sensitivity of the ion optics to the initial beam properties during the low energy beam transport. The final beam prop-
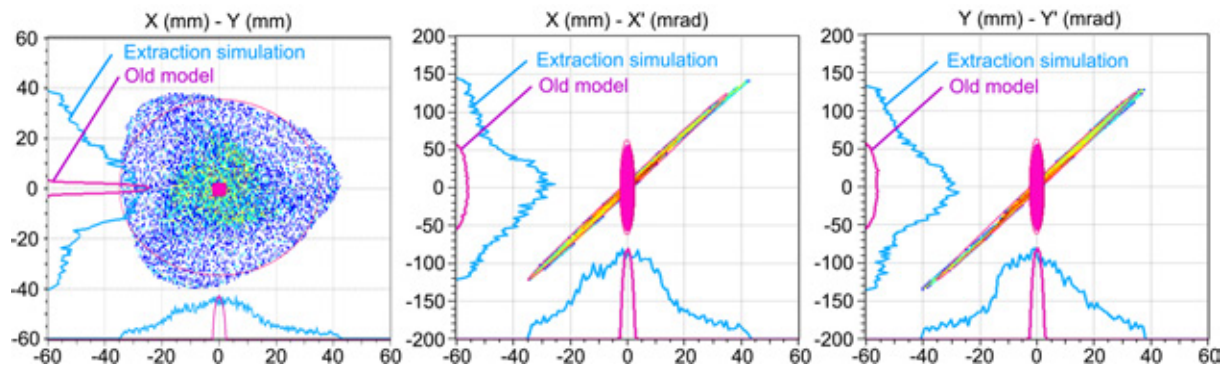
Figure 8: Comparison of the initial $^{208}Pb^{27+}$ beam definition from the extraction simulation and the initial beam used with the old Linac3 beam model. The initial transverse rms emittances are 82 mm mrad (extraction simulation) and 31 mm mrad (old model) in both transverse phase spaces. See Fig. 5 for the location.
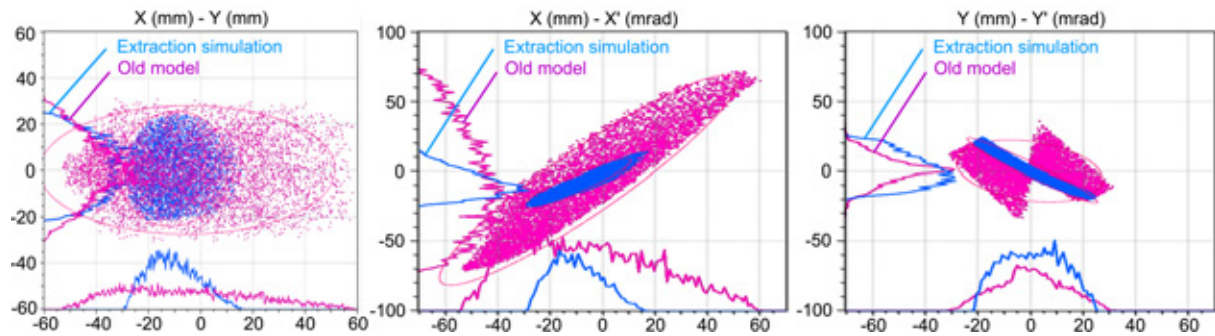

Figure 9: Comparison of the LEBT simulation results with the different initial beam definitions (see Fig. 8) at the location of the SEM grid downstream from the spectrometer (see Fig. 5). The final transverse rms emittances in (x, x') and (y, y') phase spaces are 30 and 28 mm mrad (extraction simulation) and 320 and 118 mm mrad (old model).

erties of the two cases, numerical values of which are presented in Table 1, are significantly different, and the beam properties obtained with the old initial beam definition are in strong contrast with the experimental results.

DISCUSSION

The performed ion extraction simulations provide new insight into the beam conditions and behavior in the GTS-LHC extraction system. The prediction of many signatory features observed experimentally with ECRIS ion beams and the matching of simulated beam losses and observed beam induced markings inside the extraction system increase the confidence in the simulation model. The simulations indicate that the current GTS-LHC extraction system is not fully capable of handling the high beam currents extracted during the afterglow burst. The main reason for this is the insufficient focusing properties provided by the simple extraction electrode configuration combined with the relatively long distance from the extraction to the first focusing element of the beam line. This results into significant beam losses between the extraction and the first beam line solenoid. Mitigation of these losses and consequent increase in usable ion beam current is a good motivation to continue the ion beam extraction study to improve the GTS-LHC, and Linac3, performance. Possible options to

study include a redesign of the extraction electrode geometry, implementation of a new focusing lens after the current extraction system and a redesign of the beam line section immediately after the extraction region to allow moving the first beam line solenoid closer to the ion source and reduce beam losses. These would also lead to better beam quality, which would be advantageous for beam transport and matching through the beam line elements and acceleration structures further downstream.

As the preliminary measurements in the Linac3 LEBT section indicate, the model combining the extraction and tracking simulations is promising, but not yet perfect. Further measurements are required to obtain feedback for the simulation model in order to improve it. The installation of the new pepperpot emittance meter (from Pantechnik, based on the KVI design [16, 17]) after the spectrometer, currently under commissioning and coming online in the beginning of autumn 2014, will provide improved diagnostics for this purpose. After further verification, the model will be extended to include the accelerating structures and higher energy sections of Linac3 to gain further insight into its functionality and act as a basis for future performance improvements.

ACKNOWLEDGMENT

REFERENCES

[1] L. Dumas et al., "Operation of the GTS-LHC Source for the Hadron Injector at CERN", in Proc. of ECRIS'06, Lanzhou, China, published in HEP & NP, Vol. 31, Suppl. 1, pp. 51-54 (2007). Also available as LHC Project Report 985.

[2] D. Hitz et al., "Grenoble Test Source (GTS): A Multipurpose Room Temperature ECRIS", in Proc. of ECRIS'02, Jyväskylä, Finland, pp. 53-55.

[3] D. Hitz et al., "A New Room Temperature ECR Ion Source for Accelerator Facilities", in Proc. of EPAC'02, Paris, France, pp. 1718-1720.

[4] D. Küchler et al., "Preparation of a Primary Argon Beam for the CERN Fixed Target Physics", Rev. Sci. Instrum. 85, 02A954 (2014).

[5] T. Kalvas et al., "IBSIMU: a Three-Dimensional Simulation Software for Charged Particle Optics", Rev. Sci. Instrum. 81, 02B703 (2010).

[6] J.H. Whealton et al., "Optics of Ion Beams of Arbitrary Perveance Extracted from a Plasma", J. Comput. Phys. 27, pp. 32-41 (1978).

[7] V. Toivanen et al., "Double Einzel Lens Extraction for the JYFL 14 GHz ECR Ion Source Designed with IBSimu", J. Instrum. 9, P05003 (2013).

[8] Cobham Opera Simulation Software Homepage, `http://operafea.com/`.

[9] O. Tarvainen et al., "Diagnostics of Plasma Decay and Afterglow Transient of an Electron Cyclotron Resonance Ion Source", Plasma Sources Sci. Technol. 19, 045027 (13pp) (2010).

[10] O. Tarvainen et al., "Emittance and Plasma Potential Measurements in Double-Frequency Heating Mode with the 14 GHz Electron Cyclotron Resonance Ion Source at the University of Jyväskylä", Rev. Sci. Instrum. 77, 03A309 (2006).

[11] O. Tarvainen et al., "Effect of the Gas Mixing Technique on the Plasma Potential and Emittance of the JYFL 14 GHz Electron Cyclotron Resonance Ion Source", Rev. Sci. Instrum. 76, 093304 (2005).

[12] A. Girard et al., "Electron Cyclotron Resonance Plasmas and Electron Cyclotron Resonance Ion Sources: Physics and Technology", Rev. Sci. Instrum. 75, pp. 1381-1388 (2004).

[13] R.W. Thomae et al., "Beam Experiments with the Grenoble Test Electron Cyclotron Resonance Ion Source at iThemba Labs", in Proc. of ECRIS'12, Sydney, Australia, pp. 68-70.

[14] P. Spädtke et al., "Prospects of Ion Beam Extraction and Transport Simulations", Rev. Sci. Instrum. 79, 02B716 (2008).

[15] A. Perrin and J.F. Amand, Travel User Manual, CERN (2003).

[16] H.R. Kremers et al., "A Versatile Emittance Meter and Profile Monitor", in Proc. of DIPAC'07, Venice, Italy, pp. 195-197.

[17] H.R. Kremers et al., "Comparison Between an Allison Scanner and the KVI-4D Emittance Meter", in Proc. of ECRIS'08, Chicago, USA, pp. 204-207.